

Supporting Information for

Amorphous–Crystalline CoFeB/NiPS₃ Vertical Heterostructure with Built-in Electric Field for Robust Ampere-level Water Oxidation

Sijia Zhao,^a Yaoda Liu,^{a,*} Ya Chen,^a Lei Li,^a Wenfang Zhai,^a Zhixin Guo,^a and Zhengfei Dai^{a,*}

^a State Key Laboratory for Mechanical Behavior of Materials, Xi'an Jiaotong University, Xi'an 710049, China.

*Email: ydliu0618@outlook.com (Y. L.); sensdai@mail.xjtu.edu.cn (Z. D.).

1. Calculation of turnover frequency (TOF):

$$TOF = \frac{1}{4F \times n} \quad (1)$$

In which I (A) represents the current at $\eta=300$ mV, F (~ 96485 C mol⁻¹) is the Faraday constant and n (mol) is the mole of metal atoms coated on the electrode during OER in 1M KOH. I can be evaluated with the following equation:

$$n = \frac{Q}{2F} \quad (2)$$

Here Q represent the integrated charge from the CV curve, which was obtained through electrochemical measurements in a 1M PBS electrolyte (pH=7), with a scanning rate of 50 mV s⁻¹ and a potential range of -0.2 to 0.6 V vs. RHE. As mentioned above, F is Faraday constant.

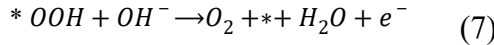
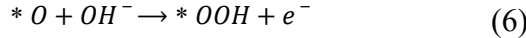
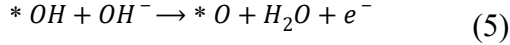
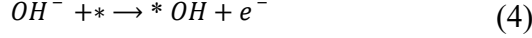
Calculation of mass activity (MA):

$$MA = \frac{j}{m} \quad (3)$$

In which j (mA cm⁻²) is the measured current density at $\eta=300$ mV, m (mg cm⁻²)=4 mg $\times 10 \mu\text{L} / 500 \mu\text{L}=0.08$ mg cm⁻².

2. DFT Calculations of OER Performance:

Under alkaline conditions, the process of OER reaction can be described by the following four steps,



in which * denotes the pure surface without adsorbed adsorbate, * O, * OH, * OOH denote the surface system with adsorbed intermediate O, OH, and OOH, respectively. The Gibbs free energy variations of the above four reaction steps are represented as ΔG_1 , ΔG_2 , ΔG_3 , and ΔG_4 , respectively.

$$\Delta G_1 = G_{*OH} + \left(\frac{G_{H_2}}{2} - 0.0592PH \right) + eU - G_* - G_{H_2O} \quad (8)$$

$$\Delta G_2 = G_{*O} + \left(\frac{G_{H_2}}{2} - 0.0592PH \right) + eU - G_{*OH} \quad (9)$$

$$\Delta G_3 = G_{*OOH} + \left(\frac{G_{H_2}}{2} - 0.0592PH \right) + eU - G_{*O} - G_{H_2O} \quad (10)$$

$$\Delta G_4 = G_{O_2} + G_* + \left(\frac{G_{H_2}}{2} - 0.0592PH \right) + eU - G_{*OOH} \quad (11)$$

U is the applied electrode potential. The standard electrode potential is 0.401 eV at pH = 14 under alkaline conditions, and the Gibbs free energy change of the determination step is $G^{OER} = \max(\Delta G_1, \Delta G_2, \Delta G_3, \Delta G_4)$, and the theoretical calculated overpotential is $\eta = G^{OER} - 0.401$. The adsorption sites are shown in Fig. S3 and the calculation results are shown in Table S1.

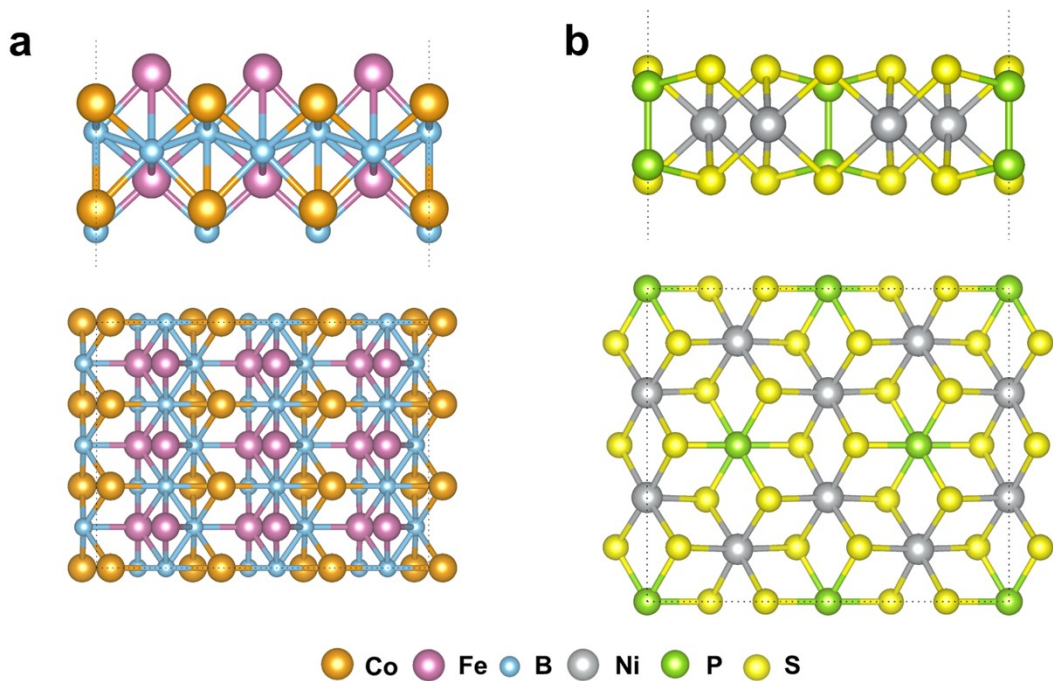


Fig. S1. Atomic models of (a) CoFeB and (b) NiPS₃.

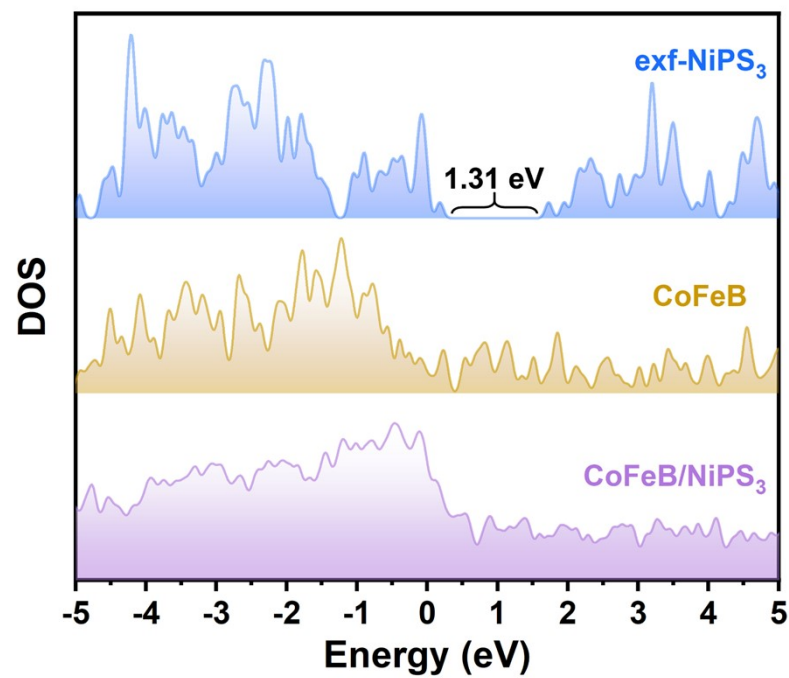


Fig. S2. DOS of CoFeB, NiPS₃, and CoFeB/NiPS₃.

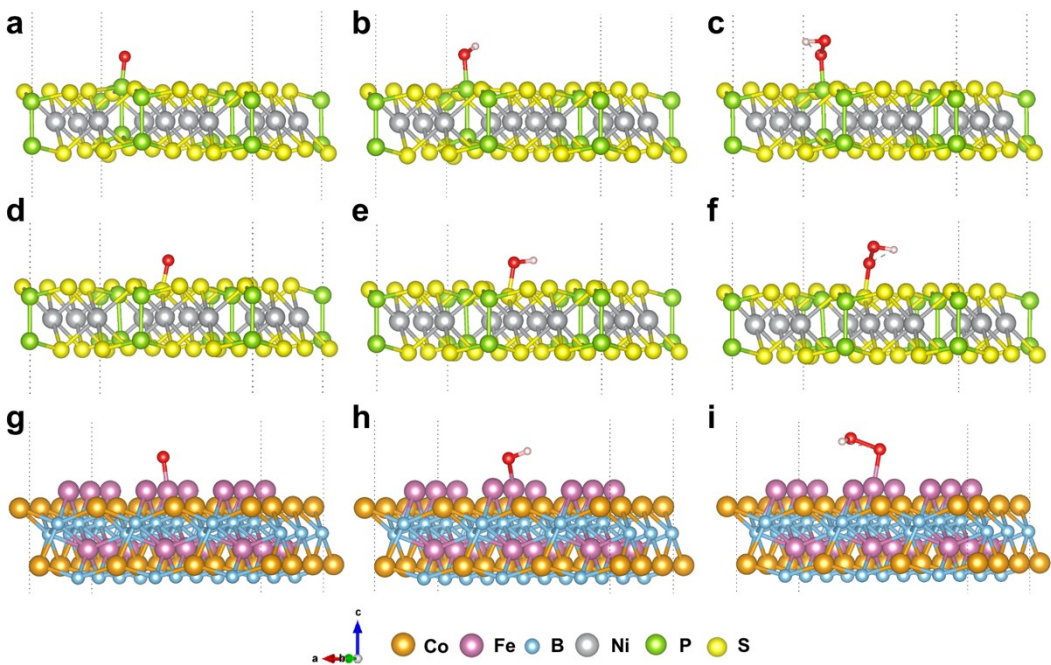


Fig. S3. The possible stable adsorption sites of *O, *OH, *OOH on the (a-c) P edge of NiPS₃, (d-f) S edge of NiPS₃, (g-i) Fe edge of CoFeB.



Fig. S4. Electrochemical cathode exfoliation process from bulk NiPS₃ to exf-NiPS₃ nanosheets.

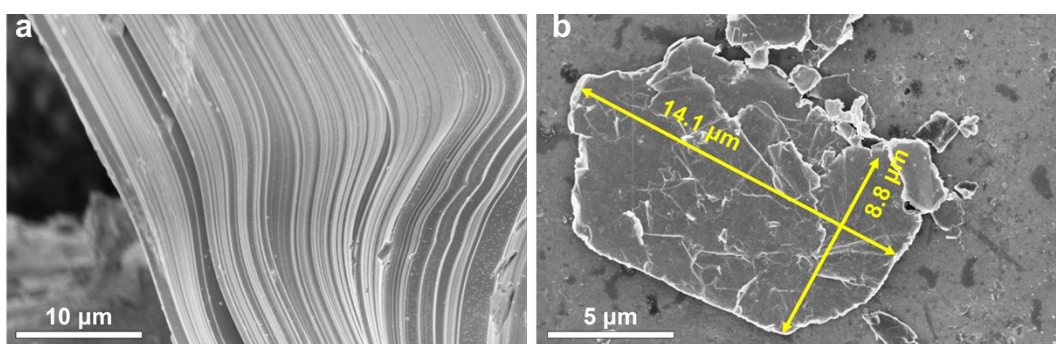


Fig. S5. SEM images of (a) the cross-section of bulk NiPS₃ and (b) exf-NiPS₃ nanosheets.

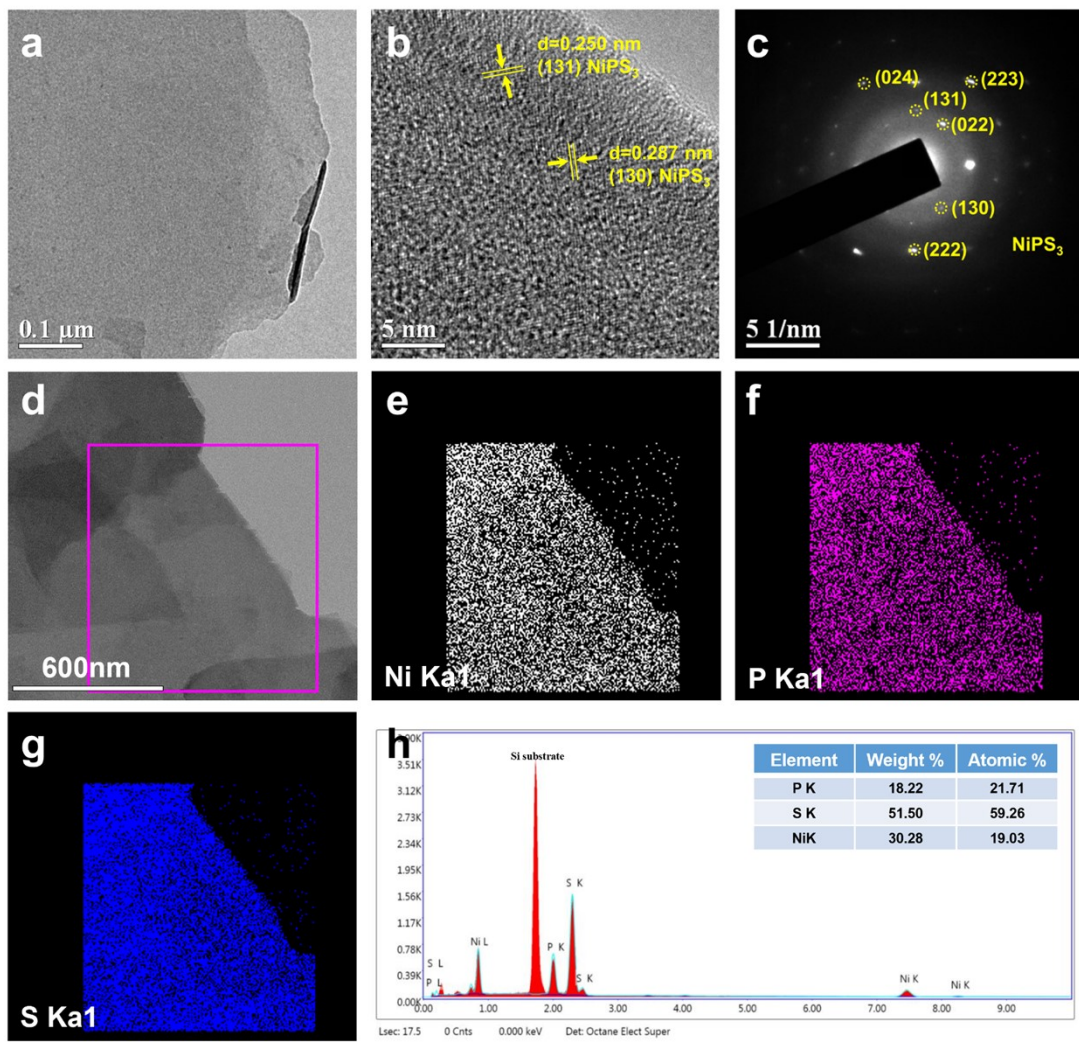


Fig. S6. (a) TEM image, (b) HRTEM image, (c) SAED pattern, (d-g) EDX mapping images, and (h) EDS spectrum of exf-NiPS₃.

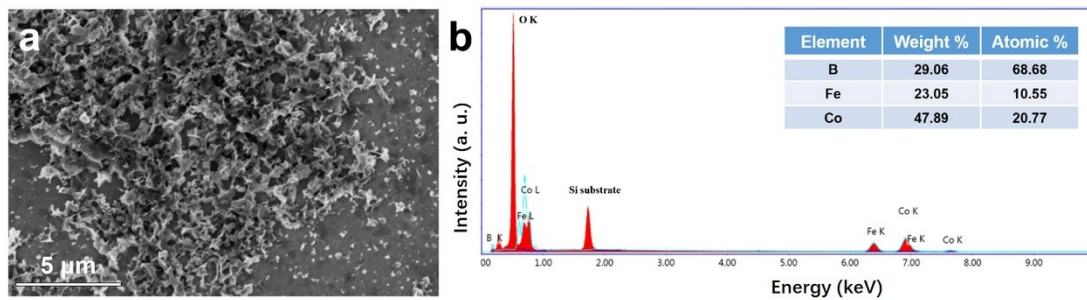


Fig. S7. (a) SEM image and (b) EDS spectrum of CoFeB.

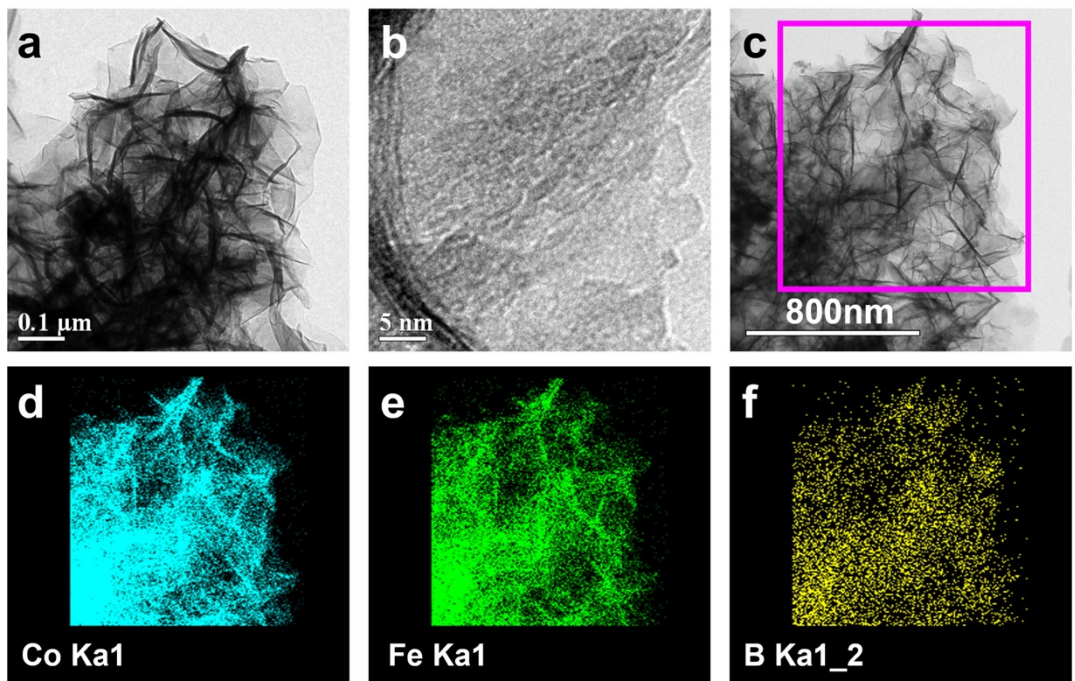


Fig. S8. (a) TEM image, (b) HRTEM image, and (c-f) EDX mapping images of CoFeB.

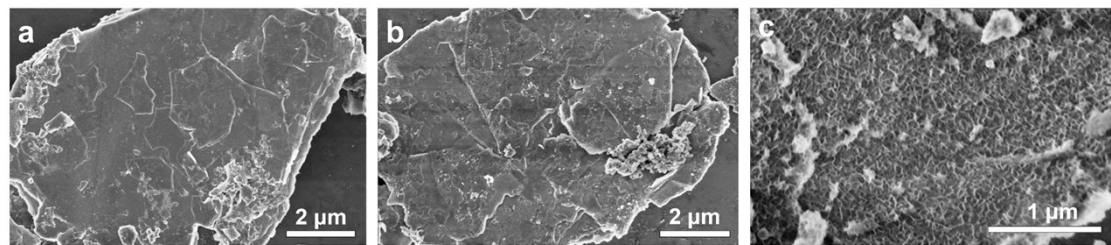


Fig. S9. SEM images of (a) CFBN-1, (b) CFBN-2 and (c) CFBN-4.

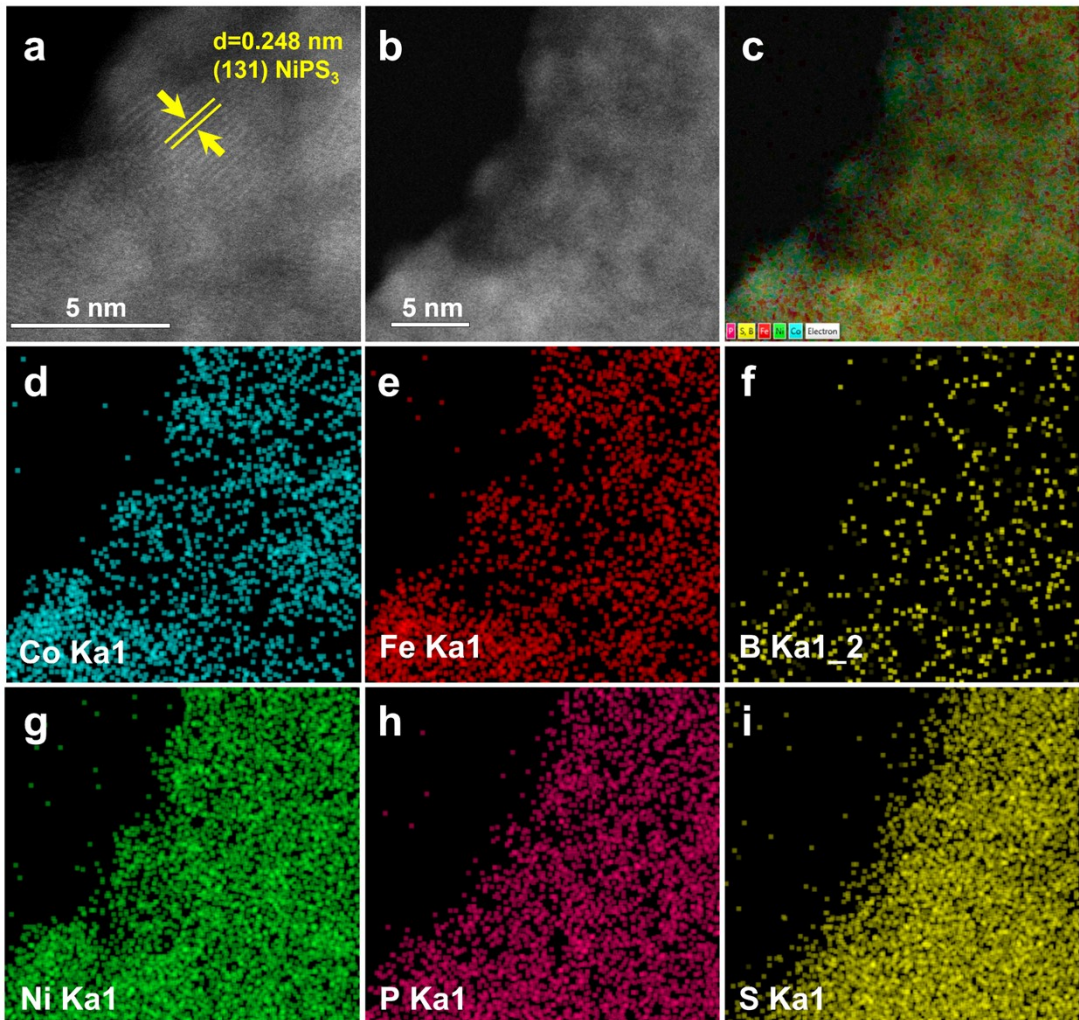


Fig. S10. (a) AC-TEM image, (b-i) EDX mapping images of CoFeB/NiPS₃.

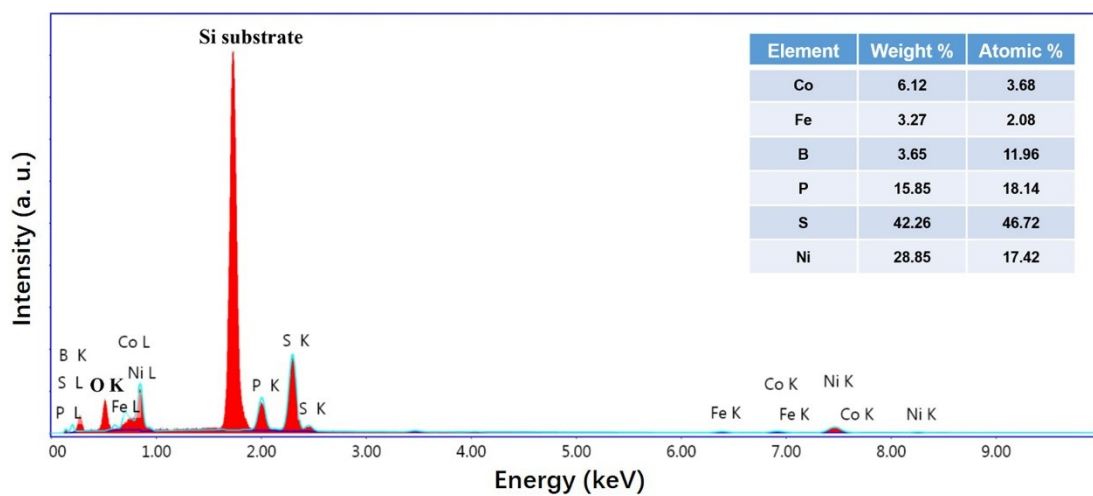


Fig. S11. EDS spectrum of CFBN-3.

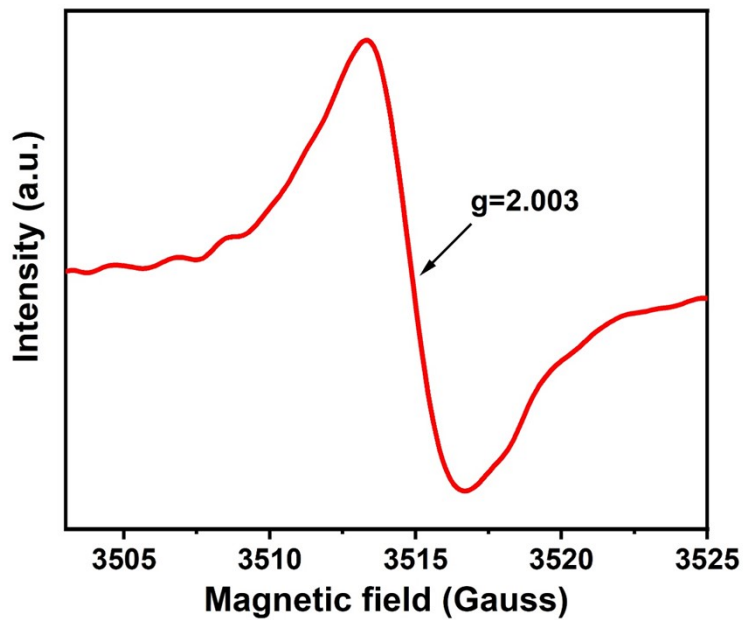


Fig. S12. The room-temperature EPR spectrum of CFBN-3 heterostructure.

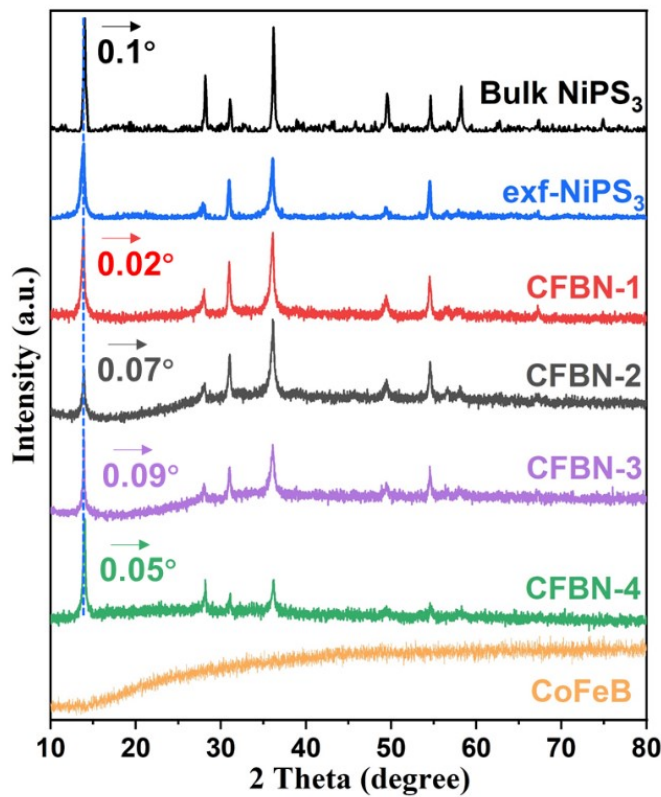


Fig. S13. XRD patterns of CFBN-1, CFBN-2, CFBN-3 and CFBN-4.

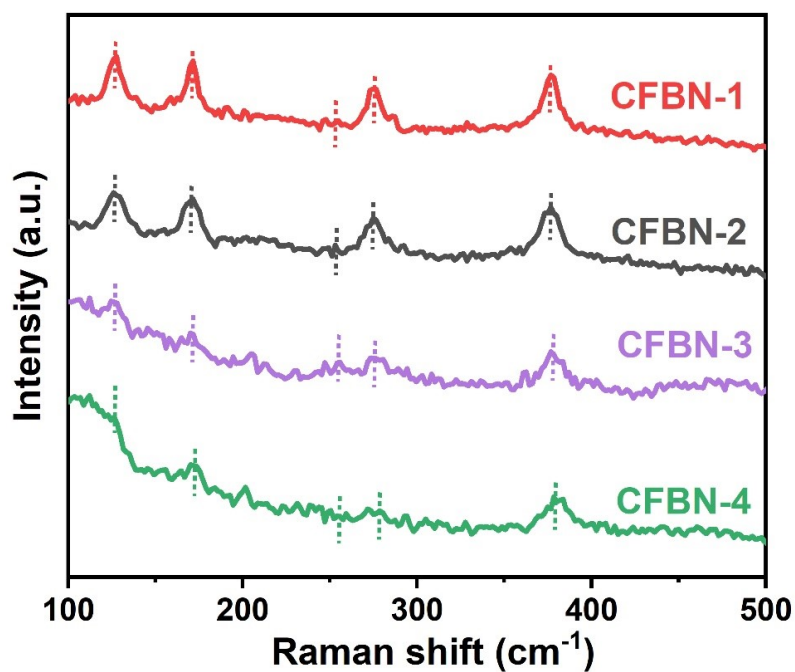


Fig. S14. Raman spectra of CFBN-1, CFBN-2, CFBN-3 and CFBN-4.

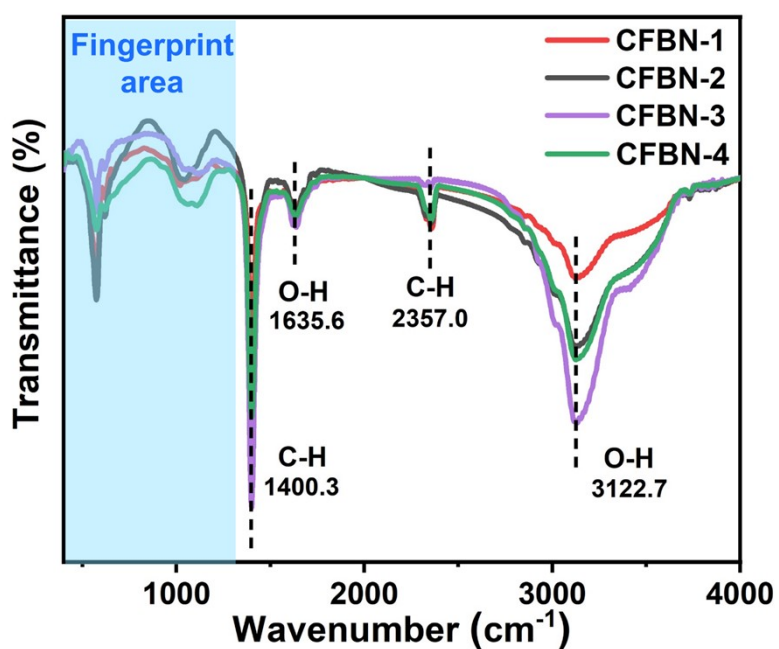


Fig. S15. FT-IR spectra of CFBN-1, CFBN-2, CFBN-3 and CFBN-4.

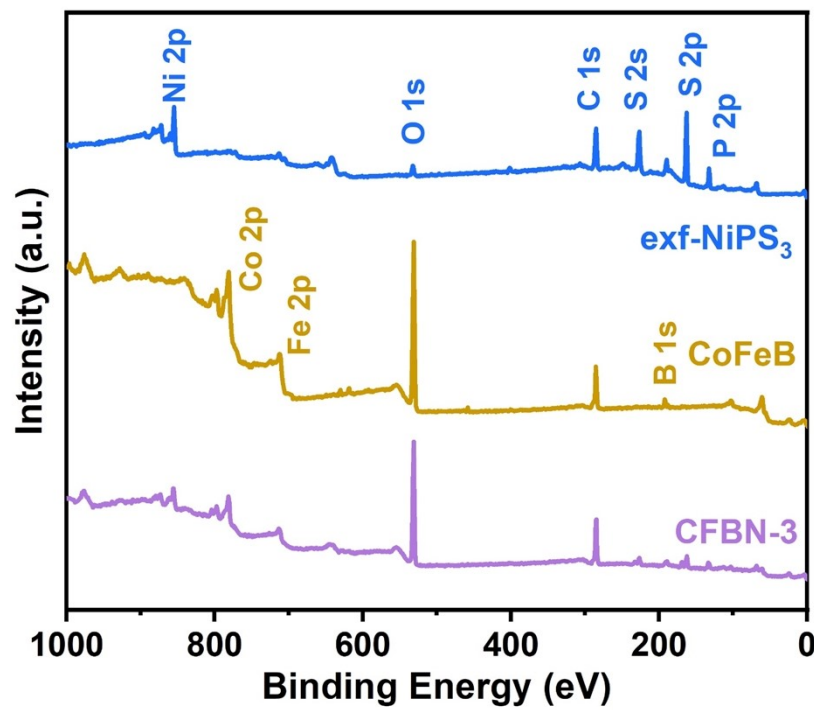


Fig. S16. XPS survey spectra of exf-NiPS₃, CoFeB and CFBN-3.

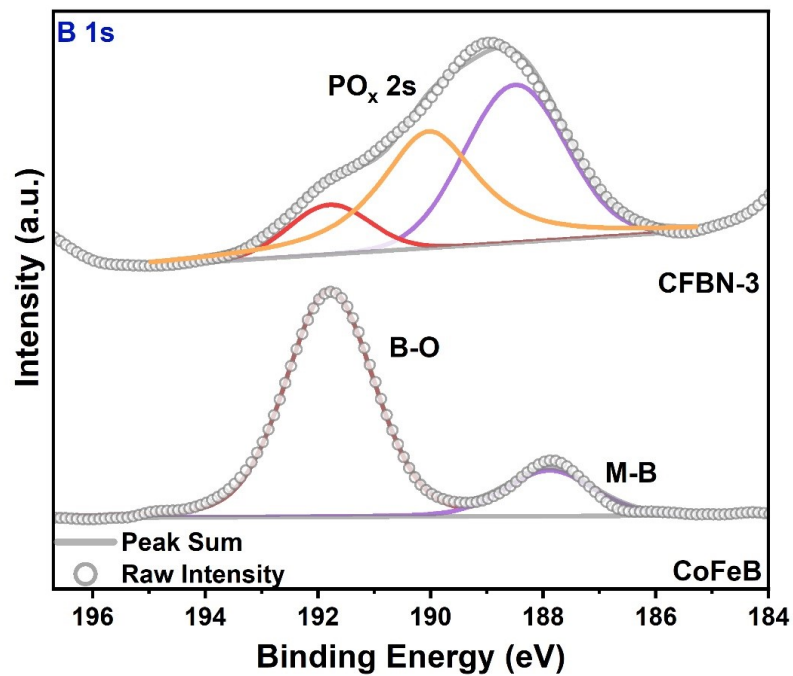


Fig. S17. B1s spectrum of CFBN-3 and CoFeB.

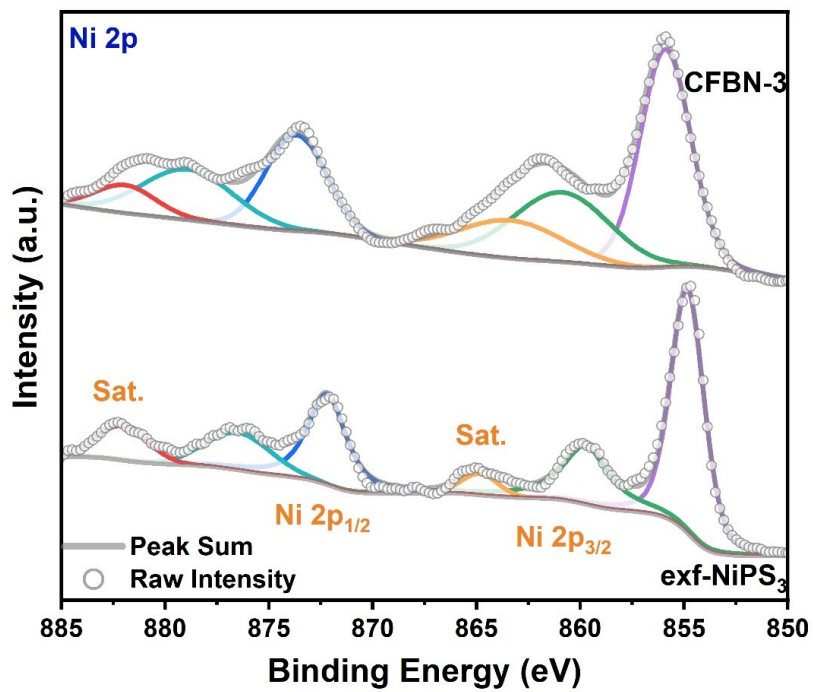


Fig. S18. Ni 2p spectra of CFBN-3 and exf-NiPS₃.

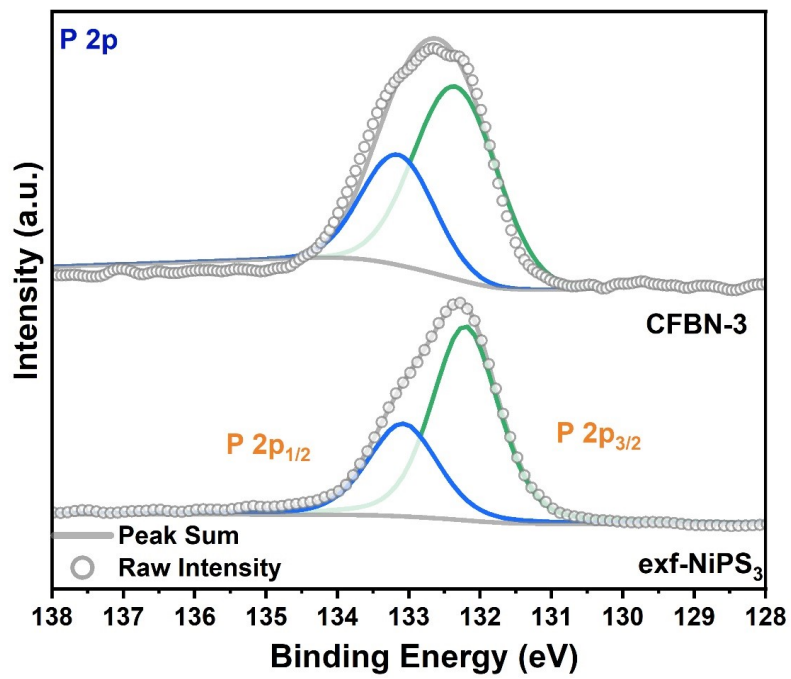


Fig. S19. P 2p spectra of CFBN-3 and exf-NiPS₃.

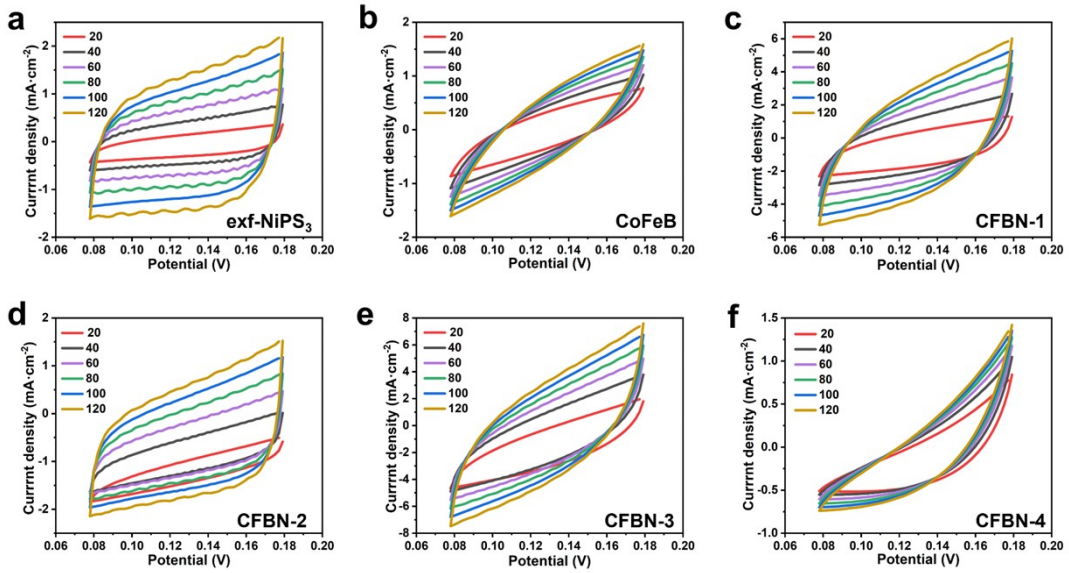


Fig. S20. The current-potential curves of samples with different scan rates for OER process in 1 M KOH: (a) exf-NiPS₃, (b) CoFeB, (c) CFBN-1, (d) CFBN-2, (e) CFBN-3, and (f) CFBN-4.

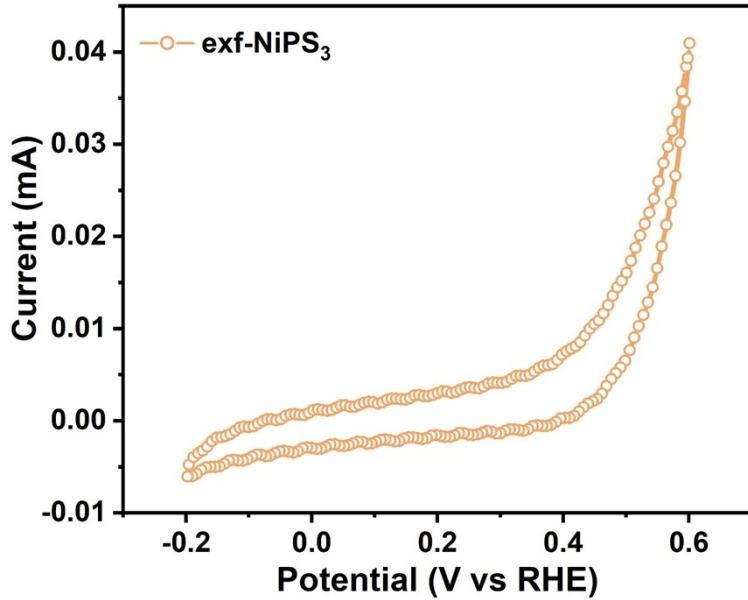


Fig. S21. CV curve for exf-NiPS₃ electrode in the potential ranges between −0.2 V vs. RHE and 0.6 V vs. RHE in 1 M PBS. The scan rate was 50 mV·s^{−1}.

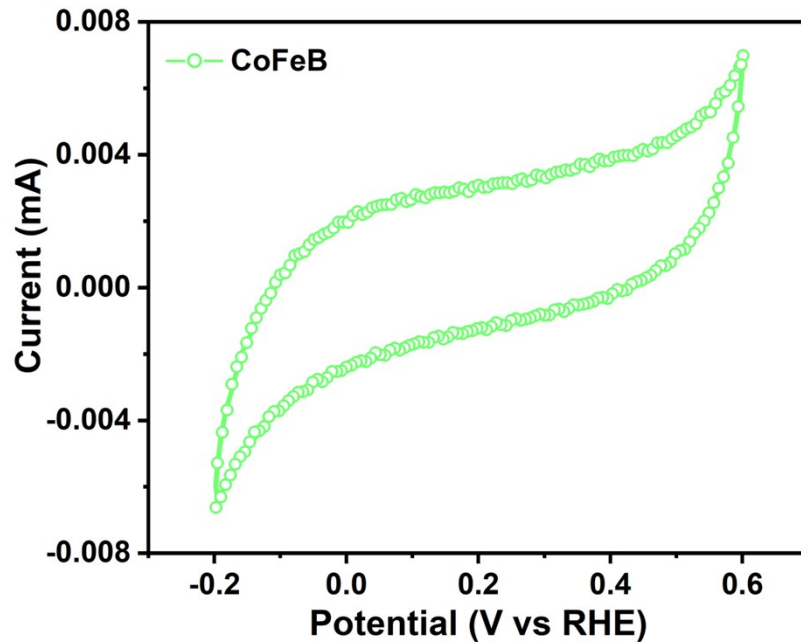


Fig. S22. CV curve for CoFeB electrode in the potential ranges between -0.2 V vs. RHE and 0.6 V vs. RHE in 1 M PBS. The scan rate was $50\text{ mV}\cdot\text{s}^{-1}$.

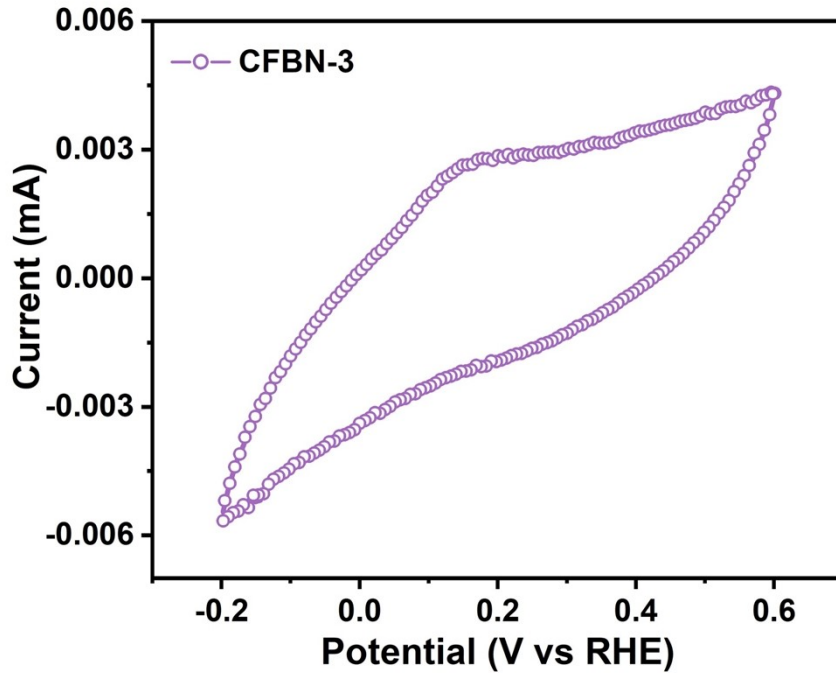


Fig. S23. CV curve for CFBN-3 electrode in the potential ranges between -0.2 V vs. RHE and 0.6 V vs. RHE in 1 M PBS. The scan rate was $50\text{ mV}\cdot\text{s}^{-1}$.

Table S1. The calculation values of OER. (calibration at 298.15 K, the unit of the physical quantity is eV, U = 0 V).

System	Site	G*	G _{H2O}	G _{H2}	G _{O2}	ΔG ₁	ΔG ₂	ΔG ₃	ΔG ₄	η
CoFeB	Fe	-453.54				-1.43	0.28	1.85	0.91	1.45
NiPS ₃	P	-205.59	-14.22	-6.8	-9.91	-0.40	-0.41	2.02	0.40	1.62
	S					1.05	-1.12	2.82	-1.14	2.42
CoFeB/NiPS ₃	Fe	-669.76				-0.78	0.42	1.31	0.65	0.91

Table S2. Comparison of the oxygen evolution reaction (OER) performance of CoFeB/NiPS₃ with that of representative catalysts of similar elements or structures in 1 M KOH.

Catalysts	η _{OER@10 mA cm⁻²} (mV)	Tafel slope (mV•decade ⁻¹)	References
MoS ₂ /NiPS ₃	296	86	1
S-FeOOH/IF	244	59	2
ZnCo ₂ O _{4-x} F _x /CNTs	350	59.2	3
Ru/Co-N-C	247	27.8	4
P-Ce SAs@CoO	261	75	5
Co-N ₄ -pyridinic SACs	351	84	6
CoNiFeMoCr	310	/	7
Ru-Co/ELCO	247	49.1	8
a-NiCo/NC	252	49	9
Porous Ni ₃ S ₄	257	67	10
Co/Fe-SNC	240	47.92	11
F-CDs/CoP/NF,	250	96	12
CoFeB/NiPS₃	235	96(50)	This work

Supplemental References

1. Y. Liu, Y. Chen, Y. Tian, T. Sakthivel, H. Liu, S. Guo, H. Zeng and Z. Dai, *Adv. Mater.*, 2022, **34**, 2203615.
2. X. Chen, Q. Wang, Y. Cheng, H. Xing, J. Li, X. Zhu, L. Ma, Y. Li and D. Liu, *Adv. Funct. Mater.*, 2022, **32**, 2112674.
3. K. Xiao, Y. Wang, P. Wu, L. Hou and Z.-Q. Liu, *Angew. Chem. Int. Ed.*, 2023, **62**, e202301408.
4. C. Rong, X. Shen, Y. Wang, L. Thomsen, T. Zhao, Y. Li, X. Lu, R. Amal and C. Zhao, *Adv. Mater.*, 2022, **34**, 2110103.
5. M. Li, X. Wang, K. Liu, H. Sun, D. Sun, K. Huang, Y. Tang, W. Xing, H. Li and G. Fu, *Adv. Mater.*, 2023, **35**, 2302462.
6. P. Kumar, K. Kannimuthu, A. S. Zeraati, S. Roy, X. Wang, X. Wang, S. Samanta, K. A. Miller, M. Molina, D. Trivedi, J. Abed, M. A. Campos Mata, H. Al-Mahayni, J. Baltrusaitis, G. Shimizu, Y. A. Wu, A. Seifitokaldani, E. H. Sargent, P. M. Ajayan, J. Hu and M. G. Kibria, *J. Am. Chem. Soc.*, 2023, **145**, 8052-8063.
7. I. A. Cechanaviciute, R. P. Antony, O. A. Krysiak, T. Quast, S. Dieckhöfer, S. Saddeler, P. Telaar, Y.-T. Chen, M. Muhler and W. Schuhmann, *Angew. Chem. Int. Ed.*, 2023, **62**, e202218493.
8. X. Zheng, J. Yang, Z. Xu, Q. Wang, J. Wu, E. Zhang, S. Dou, W. Sun, D. Wang and Y. Li, *Angew. Chem. Int. Ed.*, 2022, **61**, e202205946.
9. Z. Pei, X. F. Lu, H. Zhang, Y. Li, D. Luan and X. W. Lou, *Angew. Chem. Int. Ed.*, 2022, **61**, e202207537.
10. K. Wan, J. Luo, C. Zhou, T. Zhang, J. Arbiol, X. Lu, B.-W. Mao, X. Zhang and J. Fransaer, *Adv. Funct. Mater.*, 2019, **29**, 1900315.
11. C. Chen, M. Sun, F. Zhang, H. Li, M. Sun, P. Fang, T. Song, W. Chen, J. Dong, B. Rosen, P. Chen, B. Huang and Y. Li, *Energy Environ. Sci.*, 2023, **16**, 1685-1696.
12. H. Song, J. Yu, Z. Tang, B. Yang and S. Lu, *Adv. Energy Mater.*, 2022, **12**, 2102573.